Solution-processible electrode materials for a heat-sensitive piezoelectric thin-film sensor

Sampo Tuukkanen*[1], Tuomas Julin[1], Ville Rantanen[2], Mari Zakrzewski[1], Pasi Moilanen[3], Kaisa E. Lilja[1] and Satu Rajala[2].

[1]Department of Electronics and [2]Department of Automation Science and Engineering, Tampere University of Technology (TUT), P.O. Box 692, FI-33101 Tampere, Finland, [3]Nanoscience Center, University of Jyväskylä (JYU), P.O. Box 35, 40014 Jyväskylän yliopisto, Finland.

*Corresponding author: Sampo Tuukkanen, Tampere University of Technology, Department of Electronics, Korkeakoulunkatu 3, P.O. Box 692, FI-33101 Tampere, FINLAND, Tel: +358 40 541 5276, Fax: +358 3 3115 3394, E-mail: sampo.tuukkanen@tut.fi

Keywords: PVDF, piezoelectric sensor, printed electronics

Abstract

Piezoelectric sensors are needed in a wide range of applications from physiological measurement applications to industrial monitoring systems. Custom-designed, highly integratable and cost-effective sensor elements can be manufactured by using flexible materials in combination with high-throughput printing for fabrication. This would also enable the embedding of ubiquitous sensors in our living environment to improve the common welfare. Here, we have fabricated flexible piezoelectric sensor elements using printing methods. We demonstrated that alternative, printable electrode materials are compatible with temperature-sensitive functional substrates. Low-temperature curable electrodes were printed on both sides of unmetallized, polyvinylidene fluoride film. Various solution-processible materials – for example, carbon nanotube–cellulose composite, poly(3,4-ethylenedioxythiophene):poly(styrene sulfonate), carbon ink and silver flake ink – were used. DC sheet resistances of the electrodes and sensitivities of the sensor elements were measured. Sheet resistance varied from 10^{-1} to 10^{6} W/• and sensitivities varied from 23 to 29 pC/N. Evaporated metal electrodes as well as commercially available sensor elements were used as reference sensors. The sensing capability of printed sensors was quite insensitive to the sheet resistance of the electrodes. Further, the electrode conformation was studied by microscopy; reliability of the sensors was studied by vibration tests. In addition, sensors were tested for measuring physiological signals.

1 Introduction

Nowadays, most electronics are manufactured using conventional subtractive lithography-based processes. Use of printing technologies, however, is an additive process that has some advantages compared to subtractive processing methods. For example, as the number of process steps is decreased, the manufacturing process can be simplified. Lithographic processes contain several stages; for example, mask creation, resist deposition, exposure, development, etching, growth, evaporation, lift-off and cleaning. In printing, these steps are replaced, in the optimal case, with a single stage: printing of the desired pattern. Furthermore, the additive manufacturing process provides a more environmentally friendly process due to the decreased amount of waste. Only the required amount of material is placed in the desired location. Printing methods offer a promising path for cost-effective fabrication of ubiquitous flexible, lightweight and large-area electronics [Oea11]. A growing selection of solution-processible materials are now available and they enable printing technologies to be used for variety of applications such as flexible displays, RFID antennas, batteries and solar cells [Ari10].

Polyvinylidenefluoride (PVDF) is a piezoelectric plastic material that generates an electric charge when mechanically deformed [Ebe96, Mea10]. This makes PVDF a suitable material for thin-film pressure-sensor applications. For instance, in medical applications, the vital signals such as heart rate and respiration can be measured with a simple sensor integrated, for example, into clothing [Kär08], or into the legs of a chair or a bed [Kär09b]. A sensor matrix is capable of measuring the normal and shear stresses, which can be used to measure the pressure distribution between the foot and the shoe in order to prevent the development of pressure ulcers [Kär09a].

In commercially available sensor elements, electrodes on PVDF film have been made of metal using either Ni-Cu sputtering or screen-printing of silver ink [Mea10]. Photolithography and wet etching have been utilized to obtain complex patterns on the metallized PVDF films [Mea10]. A variety of subtractive manufacturing methods to develop a PVDF sensor matrix has been previously reported [Chi03, Wan06]. Chiu et al. used sodium hydroxide to etch away the aluminium in predesignated areas [Chi03]. Wang et al. used an excimer laser-micromachining system to pattern the electrodes on an aluminium-metallized polarized PVDF film [Wan06].

Additive manufacturing methods have been used, for example, by Pedotti et al. [Ped84] and Lee et al. [Lee03]. Pedotti et al. developed a multisensory insole for pressure-distribution measurements under the foot (pedobarography). The PVDF films were aluminium coated by vacuum evaporation through a mask obtained from a thin steel sheet by a chemical process. Lee et al. fabricated flexible organic film speakers with an ion-assisted reaction (IAR) treated PVDF as the active layer and poly(3,4-ethylenedioxythiophene):poly(styrene sulfonate) (PEDOT:PSS) materials with various organic solvents, indium tin oxide (ITO) or copper (Cu) as the electrodes. IAR was used to improve the adhesion since the highly hydrophobic surface of PVDF showed poor adhesion with other materials. Schmidt et al. have fabricated PVDF sensors containing printed PEDOT:PSS electrodes using airbrush and ink-jet techniques [Sch06]. They found a better response than for actuators constructed from sheets with metal electrodes. Since their bendable actuators operated in the extension mode, they consider the d_{13} parameter rather than d_{33}, which is measured in this paper. Very recently, Zirkl et al. demonstrated an all-printed, matrix sensor array using ferroelectric fluoropolymer P(VDF-TrFE) as the sensor material [Zir11].

Use of cost-effective printing methods for electrode fabrication on flexible PVDF film would make sensors easily integratable in versatile applications. Although metal-electrode fabrication on PVDF film using ink-jet printing has been previously demonstrated, the required high-temperature sintering step causes limitations in the sensor functionality [Kär09c]. PVDF is a thermoplastic fluoropolymer and stretching at a temperature below the melting point causes a chain packing of the molecules into the piezoelectric beta-crystalline phase [Ebe96] (see Fig. 1). The polarization direction in the crystalline film can be controlled with the simultaneous application of an electric field [Man06]. Due to the delicate fabrication procedure, the piezoelectric properties of the PVDF film are degraded when heated above 80 °C [Mea10]. PVDF films are often polled using previously fabricated electrodes, which overcomes the problem of piezoelectricity suppression during electrode curing. This type of polling may, however, introduce electrical breakdown to the PVDF. In our approach, the electrodes are not used for polling, since the materials that are used do not require a high-temperature sintering step, which would harm the piezoelectricity of the film.

To overcome the problem concerning the temperature sensitivity of the PVDF, new printable and low-temperature processible electrode materials should be considered. Carbon-based nanomaterials such as carbon nanotubes (CNT) [Niu11, Ban09], and conducting polymers such as PEDOT:PSS [Els11], are suitable materials for printed electronics since they are solution processible and compatible with flexible films. These materials can also provide both high conductivity and optical transparency, which are required in several applications [De10]. Further, these electrode materials can be used on temperature-sensitive films since they do not require subsequent heating treatments as do most metal particle-based printing inks.

Even if individual CNTs can carry currents as high as a few mA [Tuu09], relatively high contact resistances between crossing tubes limits the conductivity of randomly oriented CNT networks [Hec11]. However, flexible highly conductive electrodes have been recently obtained using, for example, networks of pure single-walled carbon nanotubes (SWCNTs) [Kae09] or a multi-walled carbon nanotube:polyaniline (MWCNT:PANI) composite [Men09]. Further, CNTs can be applied to perform more advanced functions as a hole-injection layer in organic light-emitting diodes (OLEDs) [Ban09, Ou09], or as a high surface-area material in sensors [Zou10] or supercapacitors [Kae09, Men09, Sim08]. It has been shown that cellulose derivatives are excellent dispersants for CNT [Min06]. Hence, highly viscous CNT–cellulose solutions can be obtained, which makes CNT dispersions applicable for a range of printing methods.

The manufacture of PEDOT conducting electrodes has conventionally been a challenge due to their degradation in ambient conditions [Kir05]. The PEDOT:PSS polyelectrolyte complex is the most versatile form of PEDOT due to the solution processability and stability gained [Els11]. Since PEDOT:PSS films are exceptionally transparent and conductive they have been widely applied in many different applications such as antistatic coatings, capacitors, printed circuit boards, packaging films, and as hole transport layers in OLEDs and organic photovoltaics (OPVs) [Els11].

Here we report the fabrication of electrodes on a flexible piezoelectric film, PVDF, using printing methods and various solution-processible electrode materials such as CNT–cellulose composite, PEDOT:PSS and silver flake ink, which do not require a subsequent high-temperature treatment. Evaporated metal electrodes and commercially available ready-made PVDF sensors were used as reference samples to compare their properties with the novel sensor structures. Electrical properties of the printed electrodes were characterized and the sensitivities of the sensor elements were measured. The effect of the electrode conductivity on the obtained sensor sensitivity was also analysed. Vibration-resistance tests were performed on the sensor elements since they will be exposed to vibrational stress during their use in real pressure-sensor applications. Finally, the use of sensors for physiological breathing and pulse measurements was demonstrated.

2 Materials and Methods

2.1 Printing equipment

For the electrode fabrication, a laboratory scale flexographic press (RK Flexiproof 100 from RK Print Coat Instruments Ltd.) and a bar coater (CX202 motorized bar coater purchased from mtv messtechnik oHG) were used. The bar coater (Fig. S1a in Supplementary material) was mainly used to test the printability and wettability of the ink since it is easier and faster to use than a flexographic press (Fig. S1b in Supplementary material). Electrodes were printed on both sides of the PVDF film to obtain the desired sandwich structure (Fig. 2a). The flexographic plates (Figs. 2b and c) were purchased from Espoon Painolaatta Oy. The yellow plate is a Miraclon BF plate, which has fairly good resistance to many organic solvents, and the green plate is an ASAHI DSH plate, which is suited for water- and alcohol-based inks. The plates contained 30 x 30 mm^2 squares for printing of the electrodes and narrower lines for printing quality tests. Before printing, all PVDF films were washed with isopropyl alcohol (IPA) and treated with UV ozone for 5 minutes.

Narrow lines on the edges of flexographic plates in Figs. 2b and c were used for printing quality and resolution tests. Before printing the real sensor electrodes on the PVDF, printing tests were conducted using poly(ethylene terephthalate) (PET, Melinex ST506 from Dupont Teijin films) substrate. The printing process was optimized until the successful printing of 200-mm lines was obtained both on PET and PVDF (see Fig. S6 in Supporting material).

2.2 Piezoelectric sensors

Electrode structures were printed on unmetallized 28-mm-thick uniaxially stretched and polled β-phase PVDF film (purchased from Measurement Specialities Inc.) to form piezoelectric sensors. The properties of the PVDF film provided by the supplier are presented in Table 1. An external force compressing the PVDF film introduces charges on the electrodes on different sides of the film. The piezoelectric coefficients d_{mn} and g_{mn}, charge and voltage coefficients, respectively, possess two subscripts; the first, *m,* refers to the electrical axis, while the second subscript *n* refers to the mechanical axis. Axis 1 refers to the stretching direction, axis 2 to the transverse planar direction and axis 3 to the polling axis, which is perpendicular to the material surface. Since the electrodes are on the top and at the bottom of the film, the electrical axis is always 3. Instead, the mechanical axis *n* can be 1, 2 or 3, since the stress can be applied to any of these axes. The generated surface-charge density *D* and output voltage V_0 for a PVDF sensor are defined by

$$D = Q/A = d_{3n} X_n \text{ and} \quad (1)$$

$$V_0 = g_{3n} X_n t, \quad (2)$$

where *Q* is the charge, *A* is the electrode area, X_n is the applied stress and *t* is the film thickness. [Mea10]

While the focus was on using non-metallic electrode materials to fabricate the sensor elements, more conventional metal electrodes were used in reference sensors. In-house references contain either evaporated Cu or rod-coated Ag flake ink electrodes on 28-mm-thick PVDF film. In addition, commercial reference sensors containing screen-printed Ag or sputtered Cu-Ni electrodes on 28- and 110-mm-thick PVDF films were purchased from Measurement Specialties Inc.

2.3 Inks

Various commercial and in-house solution-processible inks were used in this work. Organic as well as inorganic conducting materials were used in the inks. Conducting polymer ink made of PEDOT:PSS as well as inorganic inks made of silver flakes, CNT–cellulose composite or carbon were used.

Resistive carbon ink was purchased from Creative Materials. Carbon ink contained methyl ethyl ketone (MEK) as a solvent.

Silver flake ink Electrodag PM-460A (purchased from Henkel) has a solid content of 72 wt-% containing n-Propylacetate as the solvent. The viscosity of the ink was too high (4 Pas at 20 °C) for flexographic printing and it was therefore diluted by adding solvent. Propylene glycol monomethyl ether acetate (PGMEA) was used for dilution. After dilution, the solution was mixed using a magnetic stirrer for several hours or overnight. The formulation used for silver ink printing in this paper contained 11.9 g Electrodag PM-460A and 6.6 g PGMEA.

PEDOT:PSS inks were prepared by modifying the commercial PEDOT:PSS Clevios™ FE solution purchased from H.C. Starck GmbH. The product is a blue aqueous dispersion of PEDOT:PSS containing organic solvents and polymeric binders with a solid content of 3.0 to 4.0 wt-%. The viscosity of the commercial PEDOT:PSS solutions was modified by adding certain amounts of polyvinylpyrrolidone (PVP, purchased from Sigma-Aldrich) in IPA and/or sodium dodecyl sulphate solution (SDS, L4522 purchased from Sigma-Aldrich) in water to make it compatible for flexographic printing. PEDOT-1 ink was made by mixing 3.0 g of PEDOT:PSS solution with 0.88 g of 5 wt-% SDS in water. PEDOT-2 ink was made by mixing 3.0 g PEDOT:PSS solution with 0.20 g of 5 wt-% SDS in water and 0.31 g of 3.8 wt-% PVP solution in IPA. PEDOT-3 ink was made by mixing 2.5 g PEDOT:PSS solution with 1.88 g of IPA and 0.63 g of 3.8 wt-% PVP solution in IPA. The PEDOT:PSS ink formulations that were used are listed in Table 2.

Various formulations of nanocomposite ink containing CNTs and carboxymethylcellulose (CMC) were prepared in-house using ultrasonication. The CNT:CMC ink formulations that were used are listed in Table 3. Carbon nanotubes that were fabricated using chemical-vapour deposition were acquired from Bayer (Baytubes® C 150 P). The cellulose derivative used for CNT dispersion in this work was CMC sodium salt (Sigma-Aldrich 21904, ultra high viscosity, highly purified). The printability of the CNT:CMC composite solutions was modified by adding a certain amount of IPA and/or SDS (Sigma-Aldrich 436143, ACS reagent ≥99.0%). CNTs were first treated with concentrated HCl to remove any possible catalyst residues. CNTs were mixed with HCl and kept in a closed container overnight. Then CNTs were washed with MilliQ water until the filtrate's pH was neutral. After washing, CNTs were dried in an oven overnight at 120 °C. CMC and SDS were used as received, without any further treatment. All ink preparations were started by first mixing CNTs with MilliQ water and sonicating the mixture for 15 minutes (Sonics Vibra-Cell VCX-750 750W). For inks CNT-1, CNT-2 and CNT-4, after this initial sonication, CMC was added, mixed in ethanol, and the mixture was sonicated for an additional 25 minutes. With CNT-3, isopropanol was used instead of ethanol. CNT-5 and CNT-6 CMC was first dissolved in water for at least 24 hours and used after that. SDS was dissolved in water as concentrated stock solution and added into CNT-4, CNT-5 and CNT-6 after sonication. Dry weights were measured by drying the samples in an oven at 120 °C until the mass did not change after 30 minutes of heating.

2.4 Sheet-resistance measurement setup

The sheet resistances of printed electrodes were measured using an in-house, four-point probe setup (Fig. S2 in Supplementary material) and a multimeter (Keithley 2425 100 W SourceMeter) connected to a measurement computer equipped with a current sweep program (MATLAB software). The four probes were placed in line with equal spacing (s = 3 mm) between them. The corrected value for the sheet resistance is given by

$$R_S = G\frac{p}{\ln 2}\frac{V}{I}, \quad (3)$$

where G is the additional geometric correction factor, which depends on sample dimensions and the probe spacing [Geo11]. For the electrode structure used in this work, the geometric constant was $G = 0.9313$.

2.5 Vibration-resistance testing

Samples were tested with a Espec corp. model EV-501 vibration shaker. Samples were put through a JESD-22-B103-3 service condition 1 test. It is a test with a peak acceleration of 20 G and peak-to-peak displacement of 1.5 mm. The test starts from a minimum frequency of 20 Hz, and the frequency increases logarithmically to its maximum value of 2000 Hz and then returns logarithmically back to 20 Hz. One back and forth sweep takes four minutes and four of these sweeps were done for each sample [jed11]. During the test, samples are fixed between two aluminium plates that are 120 mm in diameter and have a 30-mm hole in the middle for the sample to vibrate freely. The aluminium plates with the sample are then attached to the vibration shaker with six screws and the test is run. The effect of the test on the sample is simply measured by comparing sheet resistances that are measured before and after the vibration test. If electrode material is detached from the sample during the test, it should increase the sheet resistance of the sample. Three PEDOT:PSS and three CNT:CMC sensor elements, all flexo-printed, underwent the vibration tests.

2.6 Structural characterization of the printed films

An optical microscope was used to characterize the overall composition of printed layers. Scanning electrode microscopy (SEM) was used to characterize the thickness and microstructure of the printed films. Before SEM-imaging, the samples were cast in epoxy and then cut and polished. Additionally, the thickness of printed films was characterized using a stylus profilometer (Veeco Dektak).

2.7 Sensitivity measurement setup

The sensitivity measurement setup has been previously reported by Kärki et al. [Kär09a]. Briefly, the normal force sensitivity is measured with a shaker generating a dynamic excitation force. A Brüel and Kjaer Mini-Shaker Type 4810 was used in the measurements. A sinusoidal input for the shaker was provided with a Tektronix AFG3101 function generator. A pretension, which produces a static force, is needed to keep the sample in place and prevent the piston jumping during the measurement. A commercial, high-sensitivity dynamic-force sensor (PCB Piezotronics, model number 209C02) and a load cell (Measurement Specialties Inc., model number ELFS-T3E-20L) were used as the reference sensors for measuring the applied dynamic and static forces. The dynamic force sensor was connected to a sensor signal conditioner (PCB Piezotronics, model 442B06) with a low-noise coaxial cable. The measurement setup is presented in Fig. S3 in the Supplementary material.

To measure the normal force sensitivity, the sensor was placed horizontally on the metal plate. A thin polyethylene terephthalate (PET) film was used under and on top of the sensor for electrical insulation. A static force of approximately 3 N between the sensor and the shaker's piston was adjusted with a position-adjustment knob. The shaker's piston was circular and 4 mm in diameter. The sensor was excited with a dynamic, sinusoidal 2 Hz input signal of 1 V_{pp}, resulting in an approximate force amplitude of 1.3 N. The excitation was done by applying the force to 9 different points on the sensor, one at a time. The same points were excited from both sides, resulting in a total of 18 excitations per sensor. The output voltage of the sensor was measured with a custom-made combination of a charge amplifier and a 16-bit AD converter. The connection to the AD converter from the sensor was provided via coaxial wires and clamp connectors. The AD converter had additional channels for sampling the voltage signals from the reference sensors. The amplification of each of the measurement channels of the converter was calibrated prior to the measurements being undertaken.

The measured data was processed to solve the sensitivity of the sensor to the force. The sensitivity was obtained by dividing the charge generated by the sensor with the force obtained with the dynamic force sensor. An example of measured sensitivity data is shown in Table S1 in the Supplementary material. Since the excitation was sinusoidal, the calculation could be done simply by dividing the amplitudes of the respective sinusoidal signals. Possible baseline drift in the signals was removed with high-pass filtering before the sinusoidal amplitudes were solved by fitting sinusoidal waveforms to the signals, as described in the IEEE Standard for Digitizing Waveform Recorders (IEEE Std. 1241) [IEE94]. The signal-to-noise ratio of each measurement of the PVDF sensors was determined based on the amplitude of the fitted sinusoidal and the RMS error of the residual after the fitting. The applied static force was solved by taking the average of the static-force sensor output during the measurement.

2.8 Physiological signal-measurement setup

The purpose was to perform proof-of-concept measurements so that the manufactured sensors would be deemed suitable for applications sensing physiological signals such as the heart rate (HR) and respiration rate (RR). Measuring mechanical cardiac activity is called ballistocardiographic (BCG) measurement and is distinct from measuring electrical cardiac activity with an electrocardiogram (ECG). However, HR information can be gained from both of the signals.

The sensor elements were attached inside a plastic folder to ensure electrical and mechanical shielding. The plastic folder was placed between two mattresses in a sofa. The test subject lay down on the mattress in a supine position. The sensors signals were amplified with a charge amplifier with the amplification of 200MV/C before digitalizing with 57 Hz sampling frequency with an ADC. Our current amplification and ADC board for pressure sensors has only four channels for simultaneous measurements. Thus, four sensors with different electrode materials were chosen for this measurement according to their performance in sensitivity measurements.

The reference measurement was performed simultaneously with a separate ADC. For the cardiac-signal reference, a single-channel ECG was recorded. For the respiration-signal reference, a flow sensor was attached under the nostrils of the test subject. A negative temperature coefficient (NTC) thermistor was used as a flow sensor. The air temperature around the NTC changes according to the person's breathing flow, thus making this an easy method for measuring breathing and causing minimal disturbance of the test subject. The signal synchronization was performed by generating a large rapid movement that could be seen in both the pressure sensors and ECG signals. The reference-sampling frequency was 800 Hz. The test person was advised to breathe normally. (Two measurements were performed: in the first, the test person was breathing normally, and in the second, the test person held her breath to allow for a better heart-signal measurement.)

While measuring BCG signals, the measured signal will contain both the cardiac and respiration activity of the test subject. For HR and RR calculations, these two signal sources need to be separated. This was performed by filtering. To gain cardiac signals, the raw signals were filtered with a band-pass filter with the cut-off frequencies at 0.5 and 2.5 Hz. This covers HRs between 30 and 150 beats per minute, which is adequate for a resting person. To gain respiration signals, the raw signals were filtered with a 0.6-Hz low-pass filter, which corresponds to 36 breaths per minute. The reference signals were filtered with a 50-Hz low-pass filter. HR and RR estimates were calculated with a peak detection algorithm and by calculating the mean distances between the successive peaks.

3 Experimental results

3.1 Sheet resistance and sensitivity

Measured sheet resistances for printed electrodes and results of the sensitivity measurements are listed in Table 4. Sheet resistances from both sides of the sensor element are averages from five different measurements with the standard deviation error. Sensitivity values are averages of 18 different measurements with the standard deviation error. The sensitivity of the sensors with the commercial, sputtered Cu-Ni electrodes on a 28-mm-thick PVDF film was left out from the results because of a very low sensitivity value, which indicates that the used sensor film was flawed.

3.2 Vibration-resistance testing

All of the tested samples passed the vibration stress test and did not show any degradation of the electrodes. Sheet resistances before and after the test stayed within the measurement error limits.

3.3 Structural characterization of the printed films

The micrographs of flexo-printed CNT:CMC and PEDOT:PSS electrodes are shown in Fig. 3. It can be observed that there are some stripes along the printing direction in both cases. The reason for this is not known. However, in the case of rod-coating, this type of stripe was not observed. The edges of printed electrodes with the various inks were quite smooth, as can be observed from Fig. S7 in the Supplementary material. In addition to this, as mentioned in section 2.1, the printing resolution of 200-mm lines was easily obtained. The electrode-edge smoothness and the high enough printing resolution prove that the fabrication method presented here is suitable for the fabrication of PVDF sensors for, for instance, plantar pressure applications.

In the SEM images, the printed electrode materials were difficult to distinguish, which is due to a poor contrast between the electrode material and the epoxy. In the case of CNT:CMC composite electrodes, it was observed that the material had moved away from the PVDF interface, maybe due to polishing or dissolving on the liquid epoxy. However, the silver flake ink contrasted well in SEM images and the thickness of the silver electrodes was 10–15 um (Fig. S4 in Supplementary material).

The structure of the printed silver-ink film looked quite granular. This was most probably due to the fact that the flakes are not melted together to form a continuous film, as in the case in high-temperature sintered Ag nanoparticle inks [Kär09c] or evaporated/sputtered metal films. This can cause decreased conductance of the Ag flake electrodes when compared with the metal electrodes' bulk silver. However, it can be seen from Table 4 that in this case the sheet resistance of the Ag flake electrode was not remarkably higher than in the other reference samples, which is most likely due to the Ag flake film being much thicker than evaporated or sputtered films.

The thickness of the printed films was very difficult to measure with the profilometer due to the roughness and curvature of the PVDF film. Only estimates could be obtained. For example, the thickness of the CNT:CMC composite film was between 100 and 300 nm.

3.4 Physiological-signal results

Due to the limitation in the number of ADC channels, four sensors with different electrode materials were chosen for this measurement according to their performance in sensitivity measurements. The measured sensors were Ag flake ink, CNT-1, CNT-5 and PEDOT-1. Ag flake ink was merely a reference for the other, more novel sensor materials.

The measured waveforms with reference signals are shown in Fig. 4a for cardiac signals and in Fig. 4b for respiration signals. The figure shows cardiac signals in a 20-second window and respiration signals in an 80-second window. It can be seen that both cardiac and respiration activity can be obtained with each sensor material. Calculated HR and RR estimates are shown on the left-hand side of each trace. It was found that the sensor placement was highly critical, as with bad positioning, no signal was gained. A slight sidewise movement of the test subject would correct this. In the shown data window, two cardiac peaks with PEDOT-1 sensor were missed, which decreases the HR estimate. In addition, one extra breath is detected with CNT-1, which increases the RR estimate. These, however, seem to be caused by the non-optimal position of the sensor rather than by sensor quality issues.

4 Discussion

4.1 Analysis of sheet-resistance results

It can be observed from the sheet-resistance results shown in Table 4 that the rod-coated CNT:CMC electrode has better reproducibility than flexo-printed electrodes. CNT:CMC electrodes printed on different sides of PVDF film using the same ink give very similar values when rod-coating was used, whereas in the flexo-printed CNT:CMC electrodes, the sheet resistance varies from one side to another. One reason for this is that the rod-coated films are thicker than flexo-printed films. In addition, our flexographic press process is not as reproducible and, thus, obtaining homogeneous films is quite difficult. For instance, a small amount of ink is used and it tends to dry quite fast on the anilox roll and block the ink cells, decreasing the ink transfer to the substrate. These problems can be solved in industrial roll-to-roll manufacturing processes where a large amount of ink is used with a continuous feed on the anilox roll and an ink-concentration monitoring system. Due to the fast-drying solvent used in Ag flake ink it was impossible to print it using flexo-printing.

The sheet resistances of different potentially transparent conductors have been previously compared by De et al. [De10]. However, they did not use printing methods for film deposition. For silver flake ink and SWNT films, they found the sheet-resistance values that were similar to what we obtained for used silver flake and CNT:CMC composite electrodes, respectively. The CNT:CMC electrodes we fabricated are only slightly transparent because the printing methods generally yield thicker films than conventional fabrication techniques. However, the flexo-printed PEDOT:PSS electrodes were highly transparent and showed the same order of magnitude in terms of sheet resistances as flexo-printed CNT:CMC electrodes. The sheet resistances obtained in this work are

low enough for some applications such as those for physiological measurements. However, if considering high-frequency applications where the effect of the sheet resistance can be crucial, high-frequency piezoelectric resonance measurements are required [Sch06].

4.2 Analysis of sensitivity results

The measured sensitivity values in Table 4 show that the obtained sensitivity is quite independent of the ink used. In addition, compared to the reference sensors, the self-made sensors have comparable sensitivities. Prominent deviations in the measured sensitivity were observed even between the measurement points of a single sensor also in the case of the reference sensors. Even if the measurements were carried out carefully in the same manner with each sensor, the sensitivity of the sensors to the shear force may be a cause for this. Even though the measurement was designed so that the shaker would only introduce stress that was normal to the sample sensor, there may have been some shear stress involved, because controlling the internal stresses of the thin and flexible PVDF material during the shaking is impossible.

The absolute value of the measured sensitivity values is somewhat smaller than that of the datasheet value for normal stress (d_{33} = −33 pC/N, shown in Table 1). This is also seen with the used reference sensors. The reasons for the difference are hard to analyse without knowing how the datasheet values have been determined. Possible shear stresses introduced in our measurement may also affect to results.

Other possible explanations for the variations in measured sensitivities are structural changes introduced to the PVDF film during the electrode-fabrication process. Various thermal, chemical and mechanical effects can take place during the electrode fabrication and cause changes in the PVDF-film conformation (see Fig. 1). Whereas metal evaporation causes a significant amount of thermal stress on the PVDF film, use of a printing process causes mostly mechanical stress due to pressing and chemical exposure due to the ink containing organic solvents. However, the possible consequences of these effects cannot be verified in the scope of this work.

In a recent work, Zirkl et al. demonstrated an all-printed active matrix sensor using ferroelectric fluoropolymer P(VDF-TrFE), similar to the PVDF material used in this work [Zir11]. The screen-printed 5-mm-thick fluoropolymer film was polled using an electric field. They obtained a sensitivity of ~30 pC/N, which is slightly higher than we found in our study.

In our case, there were some difficulties in obtaining good contacts to the sensor electrodes, which can be considered as contributing to the variance in the sensitivity values, as the varying contact resistance may affect the measurement. The contacts would not be a problem in a final application where the contact remains the same and only the applied force would change.

4.3 Sensitivity versus sheet resistance

The sensor sensitivity versus sheet resistance plot for all fabricated sensor elements is shown in Fig. S5 in the Supplementary material. One can easily observe that the sensitivity does not have a simple dependence on the sheet resistance. This suggests that the conductivity of the electrode material does not have a significant impact on the operation of the fabricated PVDF sensor during low-frequency operation. The sheet-resistance measurements and the sensitivity measurements were both carried out at low frequencies: DC and 2 Hz, respectively.

In the case of high-frequency applications, electrode conductivity plays a more important role. For instance, Schmidt et al. have studied the dependency of the dynamic piezoelectric response on the conductivity of PEDOT:PSS electrodes on a PVDF sheet [Sch06]. To analyse their experimental results, they developed an analytical model where the AC electromechanical response can be calculated by taking the finite sheet resistance of the electrode into account. Limited conductivity of the electrodes can cause, for example, loss of the signal in the case of large-area electrodes and

the drop of the signal-to-noise ratio at higher frequencies. In this work, we have only studied one size (3 cm x 3 cm) of electrodes using low-frequency pulsing, so this subject could not be fully addressed. In our sensitivity measurements, the signal-to-noise ratio was comparable with the reference sensors. Lower signal-to-noise ratios were encountered with the rod-coated sensors, and they were the only ones in which the ratios might not be acceptable for sensitive applications. The varying contact resistances were seen to be one source of decreases in the signal-to-noise ratios, since the noise amplitude was affected when the contacts were removed and reapplied. This effect could obviously be removed in target applications where the sensors can have more stable, fixed contacts to the measurement electronics.

4.4 Analysis of physiological-signal results

It can be seen in Fig. 4 that physiological signals were easily detected with all the measured sensors. It was also noted that the signal quality was dependent on how close to the chest area the sensors were placed. It was hard to position all four sensors simultaneously close enough to the chest area so that each of them would measure both cardiac and respiration signals.

The measurement setup was somewhat optimal, as the sensors were placed around the chest area of the measured subject inside the mattress. The chest area is one of the places where physiological signals are at their strongest. In applications measuring sleeping subjects, the subject could move further away from the sensors, thus, decreasing the signal strength. However, it is shown in [paa10] that physiological signals of a sleeping subject can be measured reliably even under the bed leg with pressure sensors.

5 Conclusions

Printing methods and various solution-processible materials were used in the fabrication of electrodes on a PVDF film to form piezoelectric thin-film sensors. The electrodes were characterized by measuring their sheet resistances, subjecting them to vibration testing and by analysing their structures. Additionally, the sensitivities of the fabricated sensors to force were measured. The results showed that the sheet resistances of the fabricated electrodes varied quite substantially, but that the variation did not show an observable effect on the sensitivity of the sensor. The fabricated sensors show sensitivity values comparable to the ones for commercial PVDF sensors, and, thus, can be used in the same applications. The vibration testing and structural characterization did not reveal significant limitations that would contradict this. Moreover, the sensors were successfully tested for measuring physiological signals such as heart and respiration rate from a supine test subject.

Even if the CNT–cellulose and PEDOT:PSS materials seem to work well in the sensor elements, their sheet resistances are quite low. Efforts could be put into enhancing the conductivity of these materials. For instance, one could use different thermal or chemical treatments. In addition, it has been shown that highly different conductivities can be obtained depending on which PEDOT:PSS product is used [Els11]. One interesting option to enhance electrode conductivity and transparency would be to use a composite material by mixing CNTs with PEDOT:PSS, which has been recently demonstrated [Yun11, Sch10].

One should point out that whereas rod-coating is mostly used for overall coverage of the film and printability testing, the use of flexo-printing enables customized electrode-pattern design, which is required for specific sensor applications. Further studies should include testing the reported fabrication methods in target applications such as the plantar pressure measurement [Kär09a]. Our fabrication approach also makes it easier to fabricate sensors suitable for the shear-stress measurement reported in the same study.

Acknowledgements

This research was funded by the Academy of Finland (Decision No. 138146 and 137669).

References

[Ari10] Ana Claudia Arias, J Devin MacKenzie, Iain McCulloch, Jonathan Rivnay, Alberto Salleo, Materials and applications for large area electronics: Solution-based approaches, Chem. Rev. 110 (2010) 3–24.

[Ban09] Malti Bansal, Ritu Srivastava, C. Lal, M. N. Kamalasanan, L. S. Tanwar, Carbon nanotube-based organic light emitting diodes, Nanoscale 1 (2009) 317–330.

[Chi03] S. S. Chiu, H.L.W. Chan, S. W. Or, Y. M. Cheung, P.C.K. Liu, Effect of electrode pattern on the outputs of piezosensors for wire bonding process control, Materials Science and Engineering B 99, 1–3 (2003) 121–126.

[De10] Sukanta De, Paul J. King, Philip E. Lyons, Umar Khan, Jonathan N. Coleman, Size Effects and the problem with percolation in nanostructured transparent conductors, ACS Nano 4 (12) (2012) 7064.

[Ebe96] G. Eberle, H. Schmidt, W. Eisenmenger, Piezoelectric polymer electrets, IEEE Trans. Dielectrics and Electrical Insulation 3 (1996) 624–646.

[Els11] Andreas Elschner, Wilfried Lövenich, Solution-deposited PEDOT for transparent conductive applications, MRS Bulletin 36 (2011) 794–798, doi:10.1557/mrs.2011.232.

[Geo11] Geometric factors in four-point resistivity measurement. Bulletin no. 472–13. http://www.fourpointprobes.com/haldor.html#hal. Online: Accessed 12 October 2011.

[Hec11] David S. Hecht, Richard B. Kaner, Solution-processed transparent electrodes, MRS Bulletin 36 (2011) 749–755, doi:10.1557/mrs.2011.211.

[IEE94] IEEE Standards Board (1994). IEEE Standard for Digitizing Waveform Recorders (IEEE Std 1057–1994). doi: 10.1109/IEEESTD.1994.122649.

[jed11] JEDEC STANDARD, Vibration, Variable Frequency, JESD22-B103B. http://www.jedec.org/sites/default/files/docs/22b103b.pdf. Online: Accessed 3 November 2011.

[Kae09] M. Kaempgen, C. K. Chan, J. Ma, Y. Cui, G. Gruner, Printable thin film supercapacitors using single-walled carbon nanotubes, Nano Letters 9 (5) (2009) 1872–1876.

[Kir05] S. Kirchmeyer, K. Reuter, Scientific importance, properties and growing applications of poly(3,4-ethylenedioxythiphene), Journal of Materials Chemistry 15 (2005) 2077–2088.

[Kär08] S. Kärki, J. Lekkala, Film-type transducer materials PVDF and EMFi in the measurement of heart and respiration rates. In Proceeding of the 30th Int. Conf. of the IEEE Engineering in Medicine and Biology Society, 2008, Vancouver, Canada, pp. 530–533.

[Kär09a] S. Kärki, J. Lekkala, H. Kuokkanen, J. Halttunen, Development of a piezoelectric polymer film sensor for plantar normal and shear stress measurements, Sensors & Actuators A: Physical 154 (2009) 57–64.

[Kär09b] S. Kärki. J. Lekkala, A new method to measure heart rate with EMFi and PVDF materials, Journal of Medical Engineering and Technology 33 (2009) 551–558.

[Kär09c] S. Kärki, M. Kiiski, M. Mäntysalo, J. Lekkala, A PVDF sensor with printed electrodes for normal and shear stress measurements on sole. In Proceedings of the IMEKO XIX World Congress, 2009, Lisbon, Portugal, pp. 1765–1769.

[Lee03] C. S. Lee, J. Y. Kim, D. E. Lee, J. Joo, B. G. Wagh, S. Han, Y. W. Beag, S. K. Koh, Flexible and transparent organic film speaker by using highly conducting PEDOT/PSS as electrode, Synthetic Metals 139 (2) (2003) 457–461.

[Man06] Manas Chanda, Salil K. Roy, Plastics Technology Handbook, Section: 5.4.7 Piezo- and Pyroelectric Polymers, CRC Press/Taylor & Francis Group.

[Man07] Manas Chanda, Salil K. Roy. Plastics Technology Handbook. CRC Press, Boca Raton, 4th edition, 2007.

[Mea10] Measurement Specialties Inc. Piezo film sensors. Technical manual. 86 pages. Available online at: http://www.meas-spec.com, Accessed 18 August 2010.

[Men09] C. Z. Meng, C. H. Liu, S. S. Fan, Flexible carbon nanotube/polyaniline paper-like films and their enhanced electrochemical properties, Electrochemistry Communications 11 (2009) 186–189.

[Min06] Nobutsugu Minami, Yeji Kim, Kanae Miyashita, Said Kazaoui, Balakrishnan Nalini, Appl. Phys. Lett. 88 (2006) 093123.

[Niu11] Chunming Niu, Carbon nanotube transparent conducting films, MRS Bulletin 36 (2011) 766–773, doi:10.1557/mrs.2011.213.

[Oea11] OE-A Roadmap for Organic and Printed Electronics, White Paper, 4th edition, Organic Electronics Association, 2011.
[Paa10] Paalasmaa Joonas, A respiratory latent variable model for mechanically measured heartbeats, Physiological Measurement 31(10) (2010) 1331–1344.
[Ped84] A. Pedotti, R. Assente, G. Fusi, D. De Rossi, P. Dario, C. Domenici, Multisensor piezoelectric polymer insole for pedobarography, Ferroelectrics 60 (1984) 163–174.
[Sch06] V. H. Schmidt, L. Lediaev, J. Polasik, Piezoelectric actuators employing PVDF coated with flexible PEDOT-PSS polymer electrodes, IEEE Transactions on Dielectrics and Electrical Insulation, 13 (2006) 1140.
[Sch10] S. Schwertheim, O. Grewe, I. Hamm, T. Mueller, R. Pichner, W. R. Fahrner, PEDOT:PSS layers as replacements for the transparent conductive coatings of organic solar cells, Proceedings of Photovoltaic Specialists Conference (PVSC), 2010, 35th IEEE.
[Sim08] Patrice Simon, Yury Gogotsi, Materials for electrochemical capacitors, Nature Materials 7 (2008) 845–854.
[Tuu09] S. Tuukkanen, S. Streiff, P. Chenevier, M. Pinault, H.-J. Jeong, S. Enouz-Vedrenne, C. S. Cojocaru, D. Pribat, J.-P. Bourgoin, Toward full carbon interconnects: High conductivity of individual carbon nanotube to carbon nanotube regrowth junctions, Applied Physics Letters 95 (2009) 113108.
[Wan06] Yi-Chun Wang, Ching-Hung Huang, Yung-Chun Lee, Ho-Hsun Tsai, Development of a PVDF sensor array for measurement of the impulsive pressure generated by cavitation bubble collapse, Experiments in Fluids 41 (3) (2006) 365–373.
[Yun11] Dong-Jin Yun, KiPyo Hong, Se hyun Kim, Won-Min Yun, Jae-young Jang, Woo-Sung Kwon, Chan-Eon Park, Shi-Woo Rhee, Multiwall carbon nanotube and poly(3,4-ethylenedioxythiophene): Polystyrene sulfonate (PEDOT:PSS) composite films for transistor and inverter devices, ACS Appl. Mater. Interfaces 3 (1) (2011) 43–49.
[Zir11] Martin Zirkl, Anurak Sawatdee, Uta Helbig, Markus Krause, Gregor Scheipl, Elke Kraker, Peter Andersson Ersman, David Nilsson, Duncan Platt, Peter Bodö, Siegfried Bauer, Gerhard Domann, Barbara Stadlober, An all-printed ferroelectric active matrix sensor network based on only five functional materials forming a touchless control interface, Adv. Mat. 23 (2011) 2069–2074.
[Zou10] Jianhua Zou, Jianhua Liu, Ajay Singh Karakoti, Amit Kumar, Daeha Joung, Qiang L, Saiful I. Khondaker, Sudipta Seal, Lei Zhai, Ultralight multiwalled carbon nanotube aerogel, ACS Nano 4 (12) (2010) 7293–7302.

Biographies

Sampo Tuukkanen received his Ph.D. Degree in Physics from the University of Jyväskylä in 2006. He had a two-year post-doctoral position (2007–2009) in the Molecular Electronics Group in CEA/Saclay, France, where he worked on a project that aimed at the utilization of carbon nanotubes as lines and vias in the new generation of CMOS microelectronics technology [Tuu09]. Since May 2009 he has been working as a senior researcher at the Organic Electronics Group at TUT.

Tuomas Julin is an undergraduate student in the Department of Chemistry and Bioengineering at TUT. He has been working on his master's thesis on the topic of this article since May 2011.

Ville Rantanen received his M.Sc. (Eng) Degree in Biomedical Engineering from TUT in 2007. He has worked in the Department of Automation Science and Engineering since May 2006. His research activities and interests include capacitive sensing methods for biomedical applications.

Mari Zakrzewski received her M.Sc. (Eng.) degree (with honors) in electrical engineering from TUT in 2005. Since then, she has been a Research scientist in the Department of Electronics in the Personal Electronics Group and is working towards the PhD degree. Her research interests include microwave radar monitoring of heart, ubiquitous measurement technologies, and smart home applications.

Pasi Moilanen is an undergraduate student at the University of Jyväskylä and he worked at the Nanoscience Center until the end of 2010. At the moment he works as a research scientist at nEMCel ltd, a start-up company that develops carbon-nanotube-based solutions for electromagnetic shielding, conductive inks and papers.

Kaisa Lilja received her D.Sc. (Tech.) from TUT in 2011 with the thesis “Performance, interfacial properties and applications of printed organic diodes”. She currently works as an application specialist at Biolin Scientific in Espoo, Finland.

Satu Rajala (née Kärki) received her D.Sc. (Tech.) from TUT in 2009 with the thesis “Film-type sensor materials in measurement of physiological force and pressure variables”. She has been working in the Department of Automation Science and Engineering since May 2003. Her research activities include sensor systems for physiological measurements.

TABLE 1. Properties of 28-mm-thick piezoelectric PVDF used in this work [Mea10].

Property	Symbol	Value	Unit
Thickness	t	28	10^{-6} m
Piezo Strain Constant	d_{33}	-33	10^{-12} C/N
	d_{31}	23	10^{-12} C/N
	g_{33}	-330	10^{-3} m^2/C
	g_{31}	216	10^{-3} m^2/C
Capacitance	C	380	pF/cm^2@1 kHz
Relative Permitivity	e/e_0	12 - 13	
Density	ρ	1.78	10^3 kg/m^3
Temperature Range	T	-40 to 80..100	°C

TABLE 2. List of PEDOT:PSS ink formulations used in this work.

Ink	PEDOT:PSS ink (wt-%)	PVP (wt-%)	SDS content (wt-%)	Solvent (volume ratio)
PEDOT-1	77	0	1.13	H_2O
PEDOT-2	85	0.34	0.28	H_2O:IPA in 8:1
PEDOT-3	50	0.48	0	H_2O:IPA in 0.8:1

TABLE 3. List of CNT:CMC ink formulations used in this work.

Ink	CNT:CMC mass ratio	Solid content (wt-%)	Solvent (volume ratio)	SDS content (wt-%)
CNT-1	60:40	0.8	H_2O:EtOH in 1:1	0
CNT-2	60:40	1.7	H_2O:EtOH in 1:1	0
CNT-3	50:50	1.5	H_2O:IPA in 3:1	0
CNT-4	60:40	0.8	H_2O:EtOH in 1:1	0.2
CNT-5	50:50	4.1	H_2O	0.2
CNT-6	50:50	2.4	H_2O	0.2

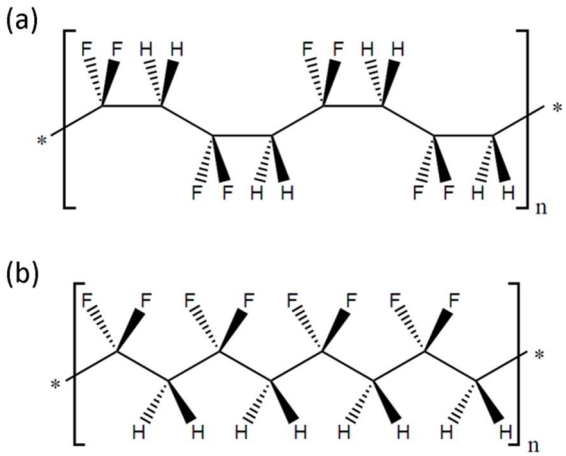

Figure 1. Structures of a) non-piezoelectric α-phase and b) piezoelectric β-phase PVDF. Figure from [Man07].

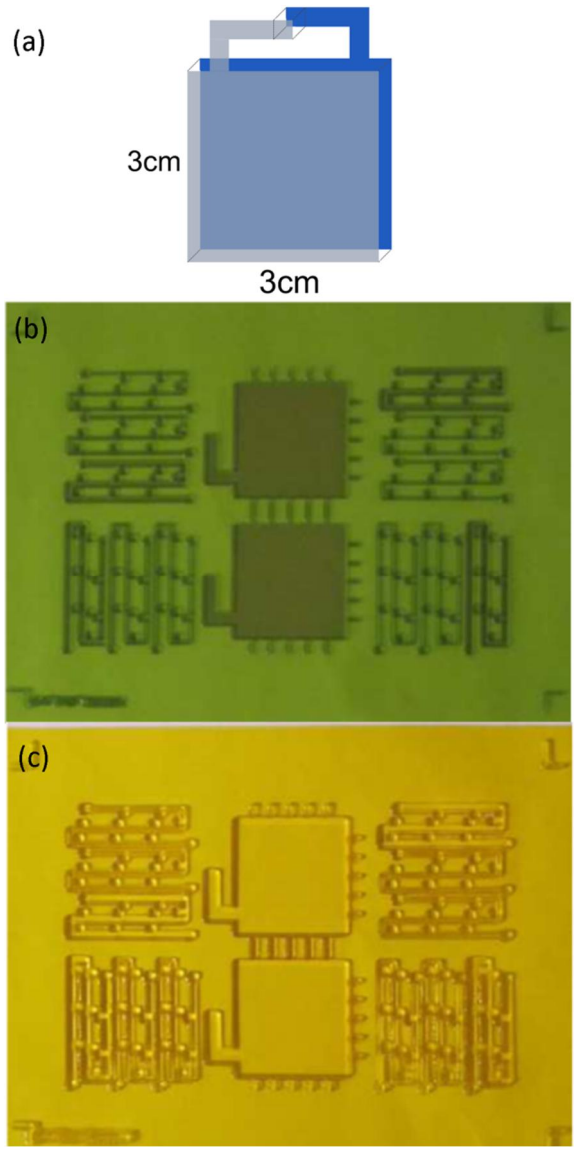

Figure 2. a) Schematic structure of the sensor element after printing on both sides of the PVDF film; b) Miraclon BF; and c) ASAHI DSH flexographic plates used for printing. Large square electrodes are used for sensor-structure printing and narrow lines for printing quality tests (in colour on the Web only).

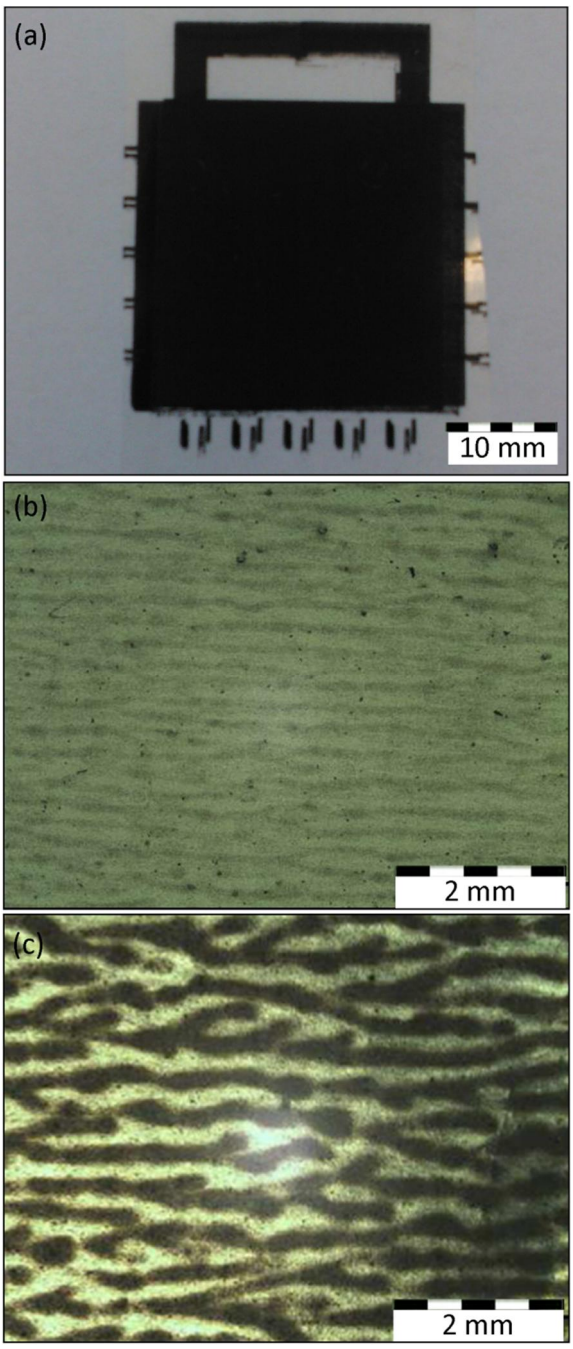

Figure 3. a) Photo of the printed carbon-ink electrodes on both sides of the PVDF film. Micrographs of the flexo-printed films of b) CNT:CMC; and c) PEDOT:PSS electrodes (in colour on the Web only).

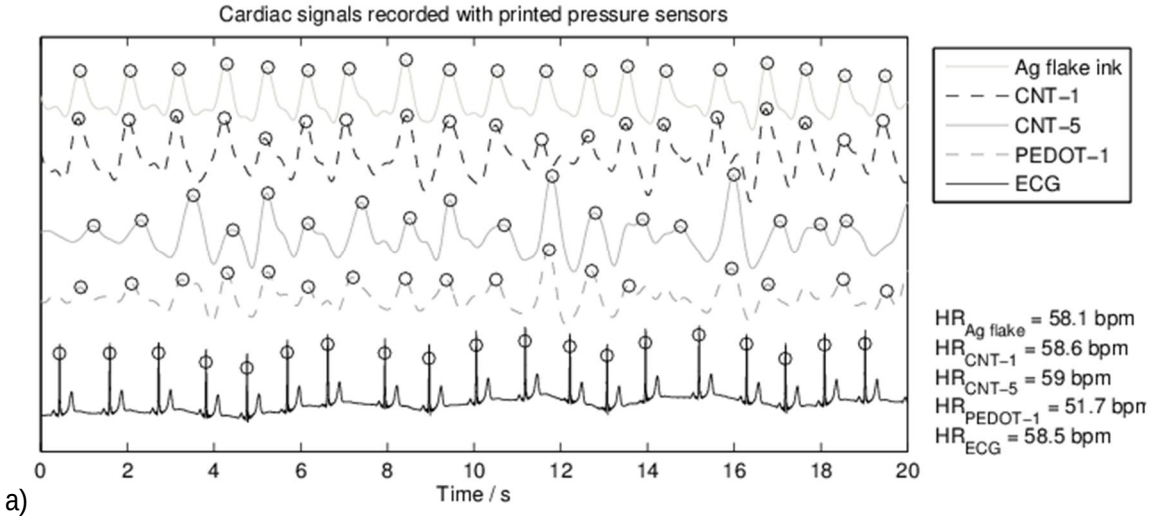

a)

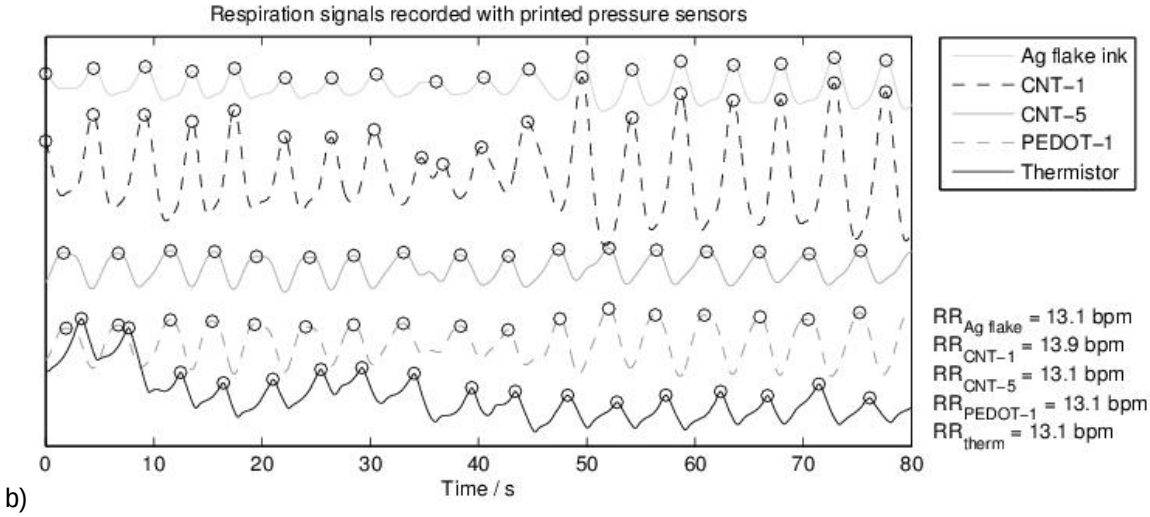

b)

Figure 4. Measured physiological signals a) for cardiac signals and b) for respiration signals.

TABLE 4. Sensitivity measurements (mean ± standard deviation). In the last reference samples, PVDF thickness is 110 mm, whereas in all the others it is 28 mm.

Ink or material	Printing or deposition method	R_S, electrode-1 (W•)	R_S, electrode-2 (W•)	Signal-to-noise ratio (dB)	Sensitivity (pC/N)
Carbon	Flexographic	$6.5 \pm 1.6 \times 10^3$	$34 \pm 17 \times 10^3$	22.4 ± 5.5	24.9 ± 1.4
CNT-1	Rod coating	$4.7 \pm 0.9 \times 10^3$	$5.3 \pm 0.9 \times 10^3$	17.9 ± 5.2	27.3 ± 2.5
CNT-2	Rod coating	$6.8 \pm 0.9 \times 10^3$	$8.1 \pm 1.9 \times 10^3$	23.2 ± 4.3	26.5 ± 1.8
CNT-3	Rod coating	$15.5 \pm 3.5 \times 10^3$	$16.0 \pm 2.8 \times 10^3$	11.4 ± 3.9	24.0 ± 2.1
CNT-4	Flexographic	$735 \pm 530 \times 10^3$	$15.9 \pm 0.9 \times 10^3$	25.5 ± 4.2	24.8 ± 1.2
CNT-5	Flexographic	$4.9 \pm 0.3 \times 10^3$	$32.7 \pm 9.7 \times 10^3$	27.4 ± 6.4	24.5 ± 0.8
CNT-6	Flexographic	$6.4 \pm 0.2 \times 10^3$	$44.7 \pm 5.0 \times 10^3$	28.8 ± 5.2	23.4 ± 3.4
PEDOT-1	Flexographic	$22.1 \pm 3.4 \times 10^3$	$49 \pm 18 \times 10^3$	27.3 ± 5.2	24.7 ± 1.8
PEDOT-2	Flexographic	$77 \pm 19 \times 10^3$	$9.5 \pm 0.8 \times 10^3$	23.2 ± 6.1	24.3 ± 2.6
PEDOT-3	Flexographic	$135 \pm 56 \times 10^3$	$160 \pm 57 \times 10^3$	28.9 ± 6.5	23.3 ± 1.6
Ag flake ink	Rod coating	0.146 ± 0.016	0.75 ± 0.16	11.1 ± 5.2	24.3 ± 2.8
Cu ref	Evaporation	1.04 ± 0.22	0.92 ± 0.08	26.2 ± 6.2	26.9 ± 1.6
Ag ink ref	Screen	0.044 ± 0.001	0.049 ± 0.001	25.6 ± 2.8	26.6 ± 0.9
Ag ink ref	Screen, 110 um	0.067 ± 0.001	0.067 ± 0.001	25.9 ± 3.0	26.1 ± 1.0
CuNi ref	Sputtering, 110um	2.14 ± 0.32	2.07 ± 0.09	23.7 ± 3.3	28.8 ± 2.5